LEAF AREA INDEX MAPPING USING RETRIEVED REFLECTANCE FROM AVIRIS DATA

Ruiliang Pu, Peng Gong and Greg S. Biging

1. INTRODUCTION

Leaf area index (LAI) has been an important driver to some ecosystem models applied at landscape to global scales. Study on the spatial distribution of LAI on the Earth's surface is helpful to understanding various biological and physical processes within a terrestrial ecosystem, such as photosynthesis, respiration, transpiration, carbon and nutrient cycle, and rainfall interception (Chen and Cihlar, 1996; Fassnacht et al., 1997; Gong et al., 1995; White et al., 1997; Hu et al., 2000). Direct measure of canopy LAI is labor-intensive and, thus, is only practicable on experimental plots of limited size. Consequently, estimating LAI over large areas is problematic (Gobron et al., 1997). Remote sensing techniques, particularly the use of satellite imagery, may offer a practical means to measure LAI at the landscape scale or even global scale (Running et al., 1989). With remote sensing techniques, scientists have made progress in developing methods that correlate remotely sensed data with regional estimates of a number of forest ecosystem variables, including LAI, absorbed fraction of photosynthetically active radiation (APAR), canopy temperature, and community type.

Since the advent of imaging spectrometers, various approaches have been developed for estimation of forest biophysical (e.g., LAI) and biochemical (e.g., chlorophyll content) parameters using hyperspectral data. They can be divided into three categories: statistical regression, physical modeling and bio-parameters mapping. So far, most attempts to estimate the LAI on the basis of airborne hyperspectral remote sensing data have relied on empirical relationships (i.e., statistical correlations) between values of LAI measured *in situ* and the values of a particular vegetation index computed from remote sensing data (e.g., Spanner et al., 1994), derivative spectra (e.g., Gong et al., 1992) or some spectral position parameters (e.g., "red edge" optical parameters, extracted from an inverse Gaussian model by Miller et al. (1990)). The physically based models rest on a theoretical basis consisting of developing a leaf scattering and absorption model that involve canopy characteristics, such as LAI (e.g., Jacquemoud et al., 1996). Imaging spectroscopy has made it possible to study the spatial distribution of biophysical and biochemical parameters because the pixel-based parametric value can be easily calculated in terms of the relationships between spectra from hyperspectral remote sensing images and biophysical and biochemical parameters measured and/or inverted from physical models (e.g., Curran et al., 1997; Hu et al., 2000). Of these three categories, empirical relationships between ground-based LAI values and various forms of multispectral and hyperspectral data are the most successful and popular. In this study, we still use the empirical regression model to predict pixel-based LAI value for LAI mapping.

The atmosphere can modify the information of the Earth's surface in several ways (Richter, 1992; Gao et al., 1993; Sturm, 1992). It contributes a signal independent of the ground (path radiance); it absorbs some fractions of the ground reflected radiance; and the atmospheric scattering (Rayleigh & aerosol) modifies the radiances of adjacent fields of different reflectance (adjacency effect). Therefore, dark areas surrounded by bright areas appear to have a higher reflectance than the intrinsic reflectance. Since the effects of atmospheric scattering and absorption on high spectral resolution remote sensing data are critical, the atmospheric correction is particularly important to imaging spectrometer data (Vane and Goetz, 1993; Green et al., 1998) for retrieval of surface reflectance and atmospheric constituents. For this reason, we will use retrieved surface reflectance to study the spatial distribution of LAI. During the 2001 EO-1 campaign in Argentina, two high spectral resolution image scenes of AVIRIS were acquired at two study sites in southern Argentina, and relevant ground truth data were collected for estimating and mapping LAI. In this study, we retrieved surface reflectance spectra from AVIRIS hyperspectral data with the atmospheric transfer code —MODTRAN4 (Berk et al., 2000). We used the retrieved pixel-based reflectance spectra to estimate and map LAI. The objectives of this study were to (1) develop an LAI mapping approach with the

Center for Assessment & Monitoring of Forest & Environmental Resources (CAMFER)
145 Mulford Hall, University of California, Berkeley, California 94720-3114, USA
Email: rpu@nature.berkeley.edu

AVIRIS hyperspectral data; and (2) compare the effectiveness of AVIRIS data at different processing stages of atmospheric correction used for estimating and mapping LAI.

2. STUDY SITES AND DATA COLLECTION

2.1 Study Sites

During the 2001 EO-1 campaign in Argentina, we set up two study sites, the south site (41º 51' 23'' S / 71º 24' 44'' W) and the north site (41º 10' 59'' S / 71º 20' 27'' W), in Rio Negro province of southern Argentina. The study areas are located on a relatively flat area, semiarid region with many patches of conifer forest plantations. The species are young- to mid-aged ponderosa pine, lodgepole pine, and Oregon pine. Besides these forest plantations, the study sites are covered by some broad-leaf species and shrub and grasses (mainly consisting of nire brush acaena, coiron, barberis, laura, rosa mosquede). The relative elevational difference within the study areas is less than 100 m and the average elevation is approximately 850 m.

2.2 Data Acquisition and Measurement

(1). AVIRIS data

At the both the north and south study sites, AVIRIS data were acquired on February 15, 2001, around 14:50 p.m. local time. The AVIRIS were acquired at an altitude of 5029 m and this led a spatial resolution of 3.6 m. A standard scene of AVIRIS image consists of 614 pixels X 512 lines X 224 bands.

(2). Spectroradiometric measurements

From March 27-29, 2001, we took reflectance measurements in the field from road surface (gravel material), bare soil, young tree canopy (ponderosa pine and lodgepole pine), grasses and shrubs using a FieldSpec®Pro FR (Analytical Spectral Devices, Inc., USA). The spectral range covered by the instrument is 350 - 2500 nm with three separate spectrometers. The first spectrometer has a spectral resolution of 3 nm while the second and the third have the same spectral resolution of approximately 10 nm. All spectra were measured at the nadir direction of the radiometer with a 25° FOV. The distance between the spectroradiometer and targets was 20 to 100 cm to allow within-target-area radiance measurement. White reference radiance was measured every 5-10 minutes. Each sample was repeatedly scanned 10 times. These spectral reflectance measurements were used for atmospheric correction for the retrieval of surface reflectance from AVIRIS data.

(3). LAI collection

An LAI-2000 Plant Canopy Analyzer (PCA) was used in the field to measure forest LAI. The PCA is based on the amount of canopy light transmittance measured across a hemispherical field by five concentrically nested sensors (Welles and Norman, 1991). The LAI measurement taken by the PCA has been termed ‘effective’ LAI because of the contamination of this measure by self-shading at the needle-to-shoot level, branch and canopy levels, and stand level (White et al., 1997; Chen and Cihlar, 1996). The operation instructions for the LAI instrument were followed carefully to ensure each LAI point measured correctly. From March 27 to 29, 2001, a total of 70 LAI measurements were taken at both sites. Each LAI measurement represents an average of ten PCA readings which were taken in an area between 100 to 1000 m^2. The locations of PCA readings in each plot were selected based on the canopy closure, age of stands and nutrient level so as to make them representative of the variability in the plot. After taking one LAI measurement, its exact location (i.e., a plot) was marked on the color composite image of AVIRIS data or on forest inventory polygon map. This has been used as references for subsequent spectral data extraction from the AVIRIS images. Since the effective LAI is less variable and easier to measure than LAI, and is also an intrinsic attribute of plant canopies (Chen and Cihlar, 1996), we directly used the effective LAI in our analysis.

3. METHODS

Figure 1 illustrates a flowchart of our analytical procedure, which consists of two parts, retrieval of surface reflectance from AVIRIS data and LAI mapping with the AVIRIS data at three different processing stages. The detailed description to the flowchart is given below.

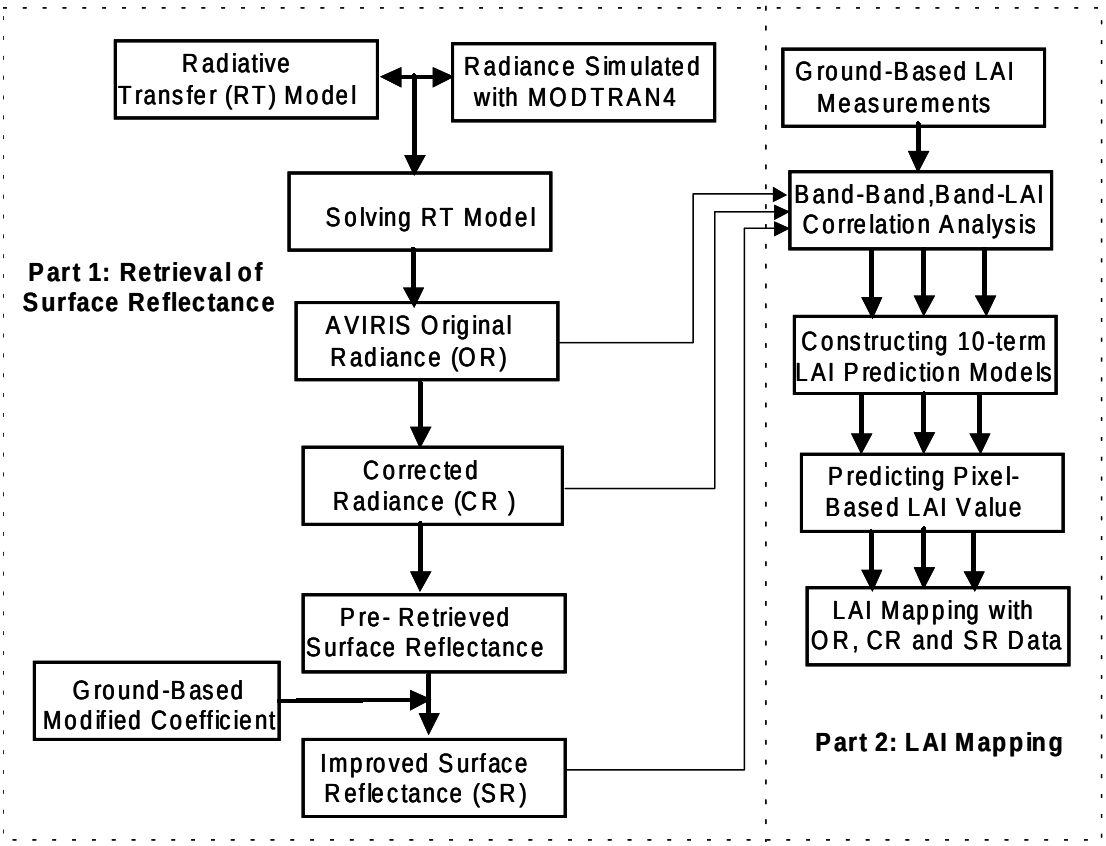

Figure 1. A flowchart of retrieval of surface reflectance and LAI mapping

3.1 Retrieval of Surface Reflectance

According to Gao et al. (1993), Sturm (1992), Green (1992) and Qu et al. (2001), a simplified radiative transfer (RT) model based on the same principles (see Tanré et al., 1986) is applied here. In a simplified form, the at-sensor radiance *L* can be a combination of the radiance reflected from Lambertian surface and scattered from atmosphere by

$$L = L_a + \frac{T_2 \rho}{1 - \rho S} \cdot \frac{E_s \cdot Cos(\theta_s)}{\pi}, \quad (1)$$

where, T_2 is the Sun-surface-sensor two-way transmittance in consideration of the total gaseous transmittance effect, L_a is the path radiance caused by atmospheric scattering, *S* is the spherical albedo of the atmosphere, ρ is the earth's surface reflectance, E_s is the exoatmospheric solar irradiance, and θ_s is the solar zenith angle. Eq. (1) can be rewritten for retrieval of surface reflectance, ρ, as

$$\rho = \frac{L - L_a}{(L - L_a)S + T_2 \cdot \frac{E_s \cdot Cos(\theta_s)}{\pi}}. \quad (2)$$

Once solving Eq. (1) for parameters, T_2, *S*, and L_a through simulation with an atmospherically radiative transfer code such as MODTRAN4 and giving a satellite measured radiance, *L*, a surface reflectance spectrum can be retrieved with Eq. (2). In this study, a procedure, as shown in Figure 1, for retrieving surface reflectance from AVIRIS data can be described as following.

Through MODTRAN4, three at-sensor total radiances were first simulated with inputs of 3 surface reflectance values (e.g., 0.0, 0.3, 0.5) and other parameter values necessary for calculating the total radiance, such as water vapor (0.7 in this experiment), aerosols, and atmospherically geographical-seasonal model. Since the water vapor is of a parameter very critical to radiance output, a principle of the "smoothness test" (Qu et al., 2001) was adopted to

determine water vapor value. The simulated output radiance was used as *L* in Eq. (1). With the three simulated at-sensor total radiances, we can solve the RT model (Eq. (1)) for parameters T_2, *S*, and L_a. Using AVIRIS image pixel value (radiance) as at-sensor radiance and the solved T_2, *S*, and L_a, we can easily calculate pixel-based surface reflectance from AVIRIS image radiances through Eq. (2). In this paper we refer to the original pixel-based radiance simply subtracted by the L_a as the corrected radiance. Since the input parameter values for MODTRAN4 cannot completely satisfy atmospheric conditions over the study sites during flight overpasses, the retrieved surface reflectance is not prefect at this stage. With a set of ratio coefficients across all spectral bands calculated by dividing the ground reflectance by the corresponding retrieved reflectance, pixel-based surface reflectance can be scaled to ground measured reflectance and improved in accuracy.

3.2 LAI Estimation and Mapping

With the AVIRIS data of three different processing stages: the original radiance (OR), corrected radiance (CR) and retrieved surface reflectance (SR), the following procedure was used in this study for LAI estimation and mapping.

Step 1. Pxel-based field spectra from 15 to 225 homogenous pixels were extracted for each of the 70 LAI measurement plots from the OR, CR and SR images. An average was taken from all pixel spectra extracted for each individual plot.

Step 2. A linear correlation coefficient is calculated between each band and the LAI measurements. The purpose of this step was to select those bands with high correlations to construct LAI prediction models.

Step 3. We selected 20 bands from the AVIRIS data of OR, CR and SR. The following band combinations were considered: (a) selecting 2 - 3 bands from each band group in terms of the correlogram (Jia and Richards, 1999); (b) selecting those bands corresponding to peak values of the correlation curve; and (c) selecting those bands with known absorption features.

Step 4. Using the piecewise regression procedure of SAS we further selected an optimal set (10 bands) of bands from the 20 bands determined at Step 3 to construct LAI prediction model. In order to evaluate the capabilities of the AVIRIS data at the three processing stages for LAI estimations, we tested the power of a regression model constructed using only 46 or 47 samples in estimating LAI values of the remaining 24 or 23 test samples. We repeated LAI model construction and estimation three times by splitting the total 70 samples into three non-overlapping test sample sets (24, 23, 23). We used all 70 samples to finally construct a 10-term prediction model for each type of the AVIRIS data to predict pixel-based LAI values for LAI mapping.

Step 5. LAI estimated from the AVIRIS data were sliced into classes and colored with a legend referencing the value ranges for each class.

3.3 Effectiveness Assessment Criteria

The capabilities of the three types of AVIRIS data for estimating LAI can be evaluated using the following three criteria:

- Multi-correlation coefficient (determination coefficient), R^2, of an LAI prediction model;
- LAI prediction accuracy evaluated based on the overall average accuracy (*OAA*) from validation samples (three sets of non-overlapping test samples), from corresponding training samples or from all 70 training samples,*OAA* is defined as

$$OAA = \left(1 - \frac{SDR}{Y_{mean}}\right) * 100.00\% \qquad (3)$$

where, $SDR = \sqrt{\frac{\sum_{i=1}^{n}(y_i - y_i)^2}{n-m-1}}$; $y_{mean} = \frac{\sum_{i=1}^{n} y_i}{n}$; $y_i (i = 1,2,..,n)$ are actual LAI measurements;

$y_i (i = 1, 2, .., n)$ are LAI values estimated from the validation samples or training samples by the constructed regression models; n is the number of samples; and m is the number of predictors in a regression model. The greater OAA is, the better is the regression result.

- Visual examination of LAI maps by comparing with a pseudo-color composite image of AVIRIS to assess the reasonability of LAI spatial distribution.

4. RESULTS AND ANALYSIS

4.1 Retrieval of Surface Reflectance

With MODTRAN4 (Berk et al., 2000), when we chose three surface reflectance values: 0.0, 0.3, and 0.5, a water vapor value of 0.7, a mid-latitude summer atmospheric geographical-seasonal model, and other necessary parameters as inputs for the code, three at-sensor total radiances were simulated for solving the simplified RT model (Eq. (1)). Figure 2 presents three total radiance curves corresponding to surface reflectance, 0.0, 0.3 and 0.5, respectively. Some absorption features along the curves of 0.3 and 0.5 reflectance, especially for those caused by water vapor, appear clearly in Figure 2. With the three simulated at-sensor total radiances and three surface reflectance values, the path radiance (L_a), the Sun-surface-sensor two transmittance (T_2), and the spherical albedo of atmosphere (*S)* could be obtained by solving the 3-equation group of Eq. (1). When replacing the simulated at-sensor radiance by the sensor image pixel value, a corrected radiance image could be produced (suppose $L_{img} \approx L$) by deducting the L_a (i.e., $L_{img} - L_a$). Further, with the two other parameters (T_2 and *S*), a retrieved surface reflectance image could be produced in terms of Eq. (1). The retrieved surface reflectance image was called as primary retrieved surface reflectance image at this stage.

Figure 3 (a-c) present atmospheric correction results at different processing stages. Figure 3 (a) is the original radiance (OR) and (b) the corrected radiance (CR) of (a). Comparing (a) with (b), we can see clearly that the atmospheric effect (scattering) influences more on the visible and near infrared region than on the longer wavelength regions. Since the surface reflectance curve is retrieved only with solved L_a, T_2 and S, there are a lot of 'spikes' along the reflectance curves, especially near 0.76 μm (O_2), 0.94 μm and 1.14 μm (H_2O), and the 2.0 μm (CO_2) absorption bands in addition to the 1.4 and 1.9 μm where water vapor absorption is strong. These might be caused by MODTRAN4 input parameters whose values are not totally adequate, especially for those sensitive gases such as water vapor. It is therefore necessary to further modify the primary retrieved reflectance with ground spectroradiometeric measurements. We used ground spectrometer data measured from road surface (high way) and plant canopy (lodgepole pine) and the primary surface reflectances retrieved from the corresponding locations on the images to calculate a set of ratio coefficients, then applied the ratio coefficients to the primary retrieved surface reflectance to obtain the final version of retrieved surface reflectance (SR) images (see Figure 3 (c)). From Figure 3 (c), it is evident that most portions of the reflectance curve are close to their ground-measured version although a few 'spikes' still remain. The 'spikes' near 0.94 and 1.14 μm indicate the water vapor effect was not completely removed. To efficiently remove the water vapor effect, a three-channel ratioing technique (Gao et al., 1993) may be tested as an alternative.

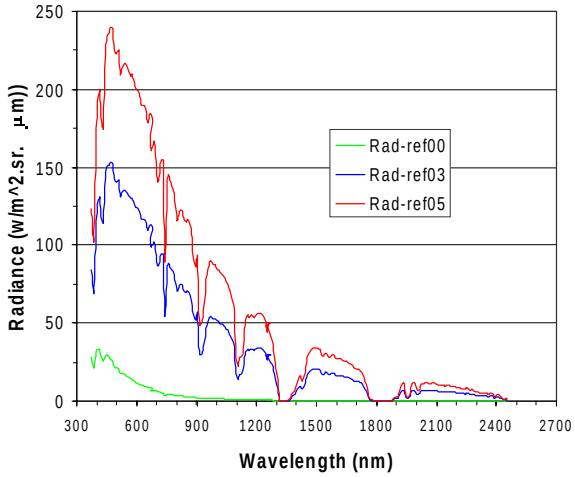

Figure 2. Total at-sensor radiance simulated using MODTRAN4 with inputs of three surface reflectances (0.0, 0.3 and 0.5) and a water vapor value of 0.7.

4.2 LAI Estimation

(1). Correlation between AVIRIS data and LAI

Linear correlations between the three types of AVIRIS data and field LAI measurements were calculated. The three correlation curves of OR, CR and SR along the wavelengths are presented in Figure 4. For AVIRIS SR data, some bands in the visible and short wave infrared (SWIR) regions have higher correlation compared to other

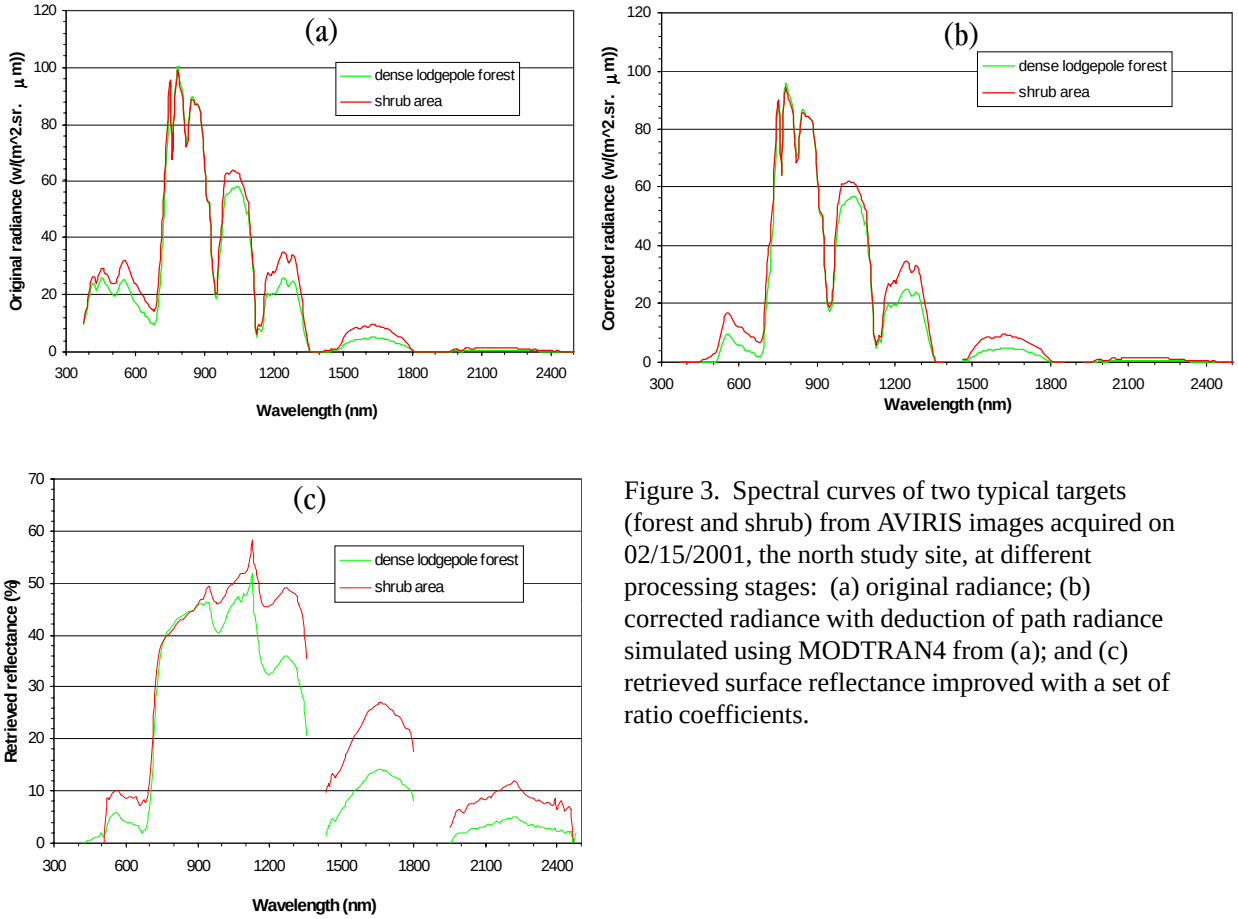

Figure 3. Spectral curves of two typical targets (forest and shrub) from AVIRIS images acquired on 02/15/2001, the north study site, at different processing stages: (a) original radiance; (b) corrected radiance with deduction of path radiance simulated using MODTRAN4 from (a); and (c) retrieved surface reflectance improved with a set of ratio coefficients.

AVIRIS data, especially in the visible region. This indicates that the atmospheric correction has effectively reduced the scattering effect of the atmosphere on the sensor data in the visible region. In the region of SWIR 2.05 – 2.4 μm, there is also a certain degree of effectiveness. However, since we have not considered a gain factor that consolidates all the multiplicative influences such as atmospheric transmission, solar irradiance and instrument response (Goetz et al., 1997), a simple deduction of the effect of atmospheric path radiance from the OR data has not improved the correlation. For all the three types of data, the SWIR bands can be used as a potential range for LAI estimation because the effect of atmosphere is relatively weak in this region except two strong water absorption bands centered near 1.4 and 1.9 μm.

(2) LAI prediction models

In order to construct LAI prediction models, we first selected 20 relatively important bands from all AVIRIS bands according to the three criteria mentioned earlier. Using the piecewise regression procedure from SAS, an optimal set (10 bands) of bands from the 20 bands was selected to construct LAI prediction models for the three types of AVIRIS data. The optimal number of bands selected was determined based on Figure 5. When all three types of data were considered, 10 bands were sufficient because the R^2 almost no longer increases if more bands were used. Therefore, we used all 70 samples to finally construct one 10-term prediction model for each type of the data. Table 1 lists some indices for model evaluation and band wavelengths selected for each type of data. Note that all spectral data selected were transformed into logarithmic values. All model indices including R^2, overall accuracy (OAA) and standard deviation (SD) show that the AVIRIS SR data are the best among the three. This indicates that the atmospheric correction executed to OR data and the procedure of retrieving surface reflectance are helpful in estimating forest LAI. According to Curran (1989), most of the bands used relate to biochemical absorption features and account for biological significance because canopy LAI is considered to have a direct or indirect relation with most of the biochemical absorption features. For example, 2 - 3 bands selected for each type of the data (539 and 626 nm for OR; 539, 558 and 626 nm for both CR and SR) locate in the visible region and, therefore, can relate to the chlorophyll absorption features; most of the other bands in the SWIR region are affected by water, protein,

nitrogen, starch, oil, lignin, and cellulose absorption features (1080, 1174, 1274, 1653, 1763, 1792 and 2221 nm); and only 780 nm for all three types of the data and 2420 nm for SR seem to have no causal association with those known absorption features (> 50 nm away). Among the three types of data, there are 6 common bands (539, 626, 780, 1763, 1792, and 2221 nm). We regard these 6 common bands more important than the others in the selected 20-band group.

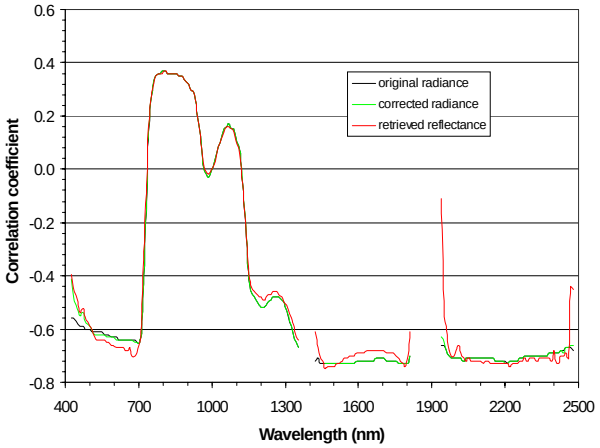

Figure 4. Comparison of correlation coefficients among the AVIRIS data at the three different processing stages: original radiance, corrected radiance and retrieved surface reflectance.

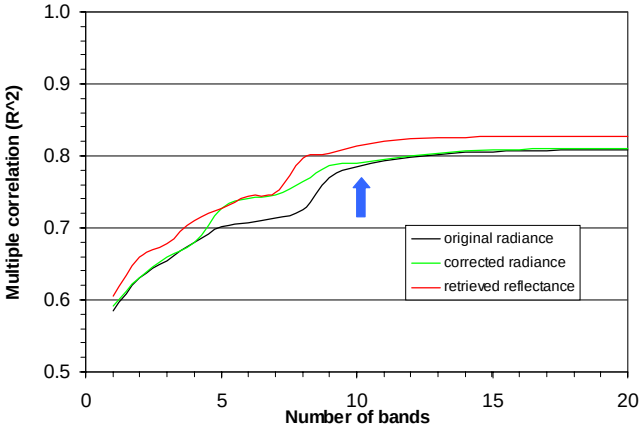

Figure 5. R^2 value varying with the increase of the number of bands included in a regression model.

(3). Test of LAI prediction models

Table 2 lists evaluation indices of training (from 46 or 47 samples) and test sets (remaining 23 or 24 samples) for the three types of data. All results listed were obtained through averaging the results from training or testing. All indices for AVIRIS SR are better than those of the other two (OR and CR) with training samples. For the results obtained from the test sets, it seems that atmospheric correction did not improve the accuracy of LAI estimation. In fact, the accuracies for CR and SR data are lower by a little bit than those of OR data. This may have two explanations: the atmospheric correction is insignificant; or the results are inconclusive because the training and test

Table 1. LAI prediction models (10-term) of the three types of AVIRIS data, original radiance (OR), corrected radiance (CR), and retrieved surface reflectance (SR). N = 70 samples

	Logarithm of OR	Logarithm of CR	Logarithm of SR
R^2	0.7854	0.7904	0.8130
Wavelengths (nm)	539 626 780 1080 1174 1274 1653 1763 1792 2221	539 558 626 780 1080 1212 1274 1763 1792 2221	539 558 626 780 1174 1653 1763 1792 2221 2420
OAA (%)	76.63	76.91	78.19
SD	0.5677	0.5609	0.5297

Note: All of R^2 are significant at 0.99 confident level; OAA-overall average accuracy; SD-standard deviation

Table 2. Comparison of the effectiveness of LAI estimation with 10-term regression models from the three types of AVIRIS data. 46 or 47 training samples and 24 or 23 test samples were used. All test results were obtained through averaging the three non-overlapping test sets.

Effectiveness indiex		Logarithm of OR	Logarithm of CR	Logarithm of SR
Training set	R^2	0.8119	0.8225	0.8306
	OAA(%)	78.24	78.88	79.34
	SD	0.5283	0.5125	0.5020
Test set	OAA(%)	67.19	62.33	66.71
	SD	0.7931	0.9232	0.8126

Note: All of R^2 are significant at 0.99 confident level; OAA-overall average accuracy; SD-standard deviation

sample sizes are not big enough. Nevertheless, based on the results shown in Table 1, the retrieved surface reflectance data should be expected to have the potential to improve the accuracy of LAI estimation compared to the use of OR or CR data. The expectation can also be supported by LAI mapping result analyzed below.

4.3 LAI Mapping

A unique color or a gray level was assigned to a class of pixel-based LAI value, and corresponding legend was also added onto the pixel-based LAI maps. These LAI maps reflect spatial distribution of different LAI classes (see Figure 6). Figure 6 consists of 8 parts of the two study sites (N – north site and S – south site): (a-N, -S) are false-color composite images with AVIRIS bands 45 (NIR), 24 (Red), and 12 (Green); (b-d, -N and -S) are LAI maps mapped using AVIRIS OR, CR and SR, respectively. For the false color composite images the areas with the highest LAI are in red color while the lowest LAI in blue-green-white color and the medium LAI in reddish and dark-red colors. Compared to the false color composite images, the LAI maps produced by SR are the most reasonable because the spatial distribution of LAI patches on the maps matches the false color image very well, and the maps reflect detailed LAI variation, especially for patches at the low and high ends of LAI when compared with those from the CR and OR. From Figure 6 (a-N, -S), it is evident that the range of LAI mapped from the OR is narrow. For LAI maps produced from CR, they are better than those from the OR, but, obviously, worse than those with the SR. This could be due to the results of atmospheric correction and use of the retrieved surface reflectance.

5. SUMMARY AND CONCLUSIONS

In this study, we compared the effectiveness of AVIRIS data processed at three levels for LAI estimation. The three data levels are original radiance (OR), corrected radiance (CR) and retrieved surface reflectance (SR) images. AVIRIS images were acquired on February 15, 2001 at the north and south study sites during an EO-1 campaign in Argentina. Spectraoradiometric measurements were taken from road surface, vegetation and bare soil with a FieldSpec®Pro FR spectrometer. A total of 70 LAI measurements with an LAI-2000 Plant Canopy Analyzer were also taken in the field. We first simulated the total at-sensor radiances using MODTRAN4. Then, we solved a

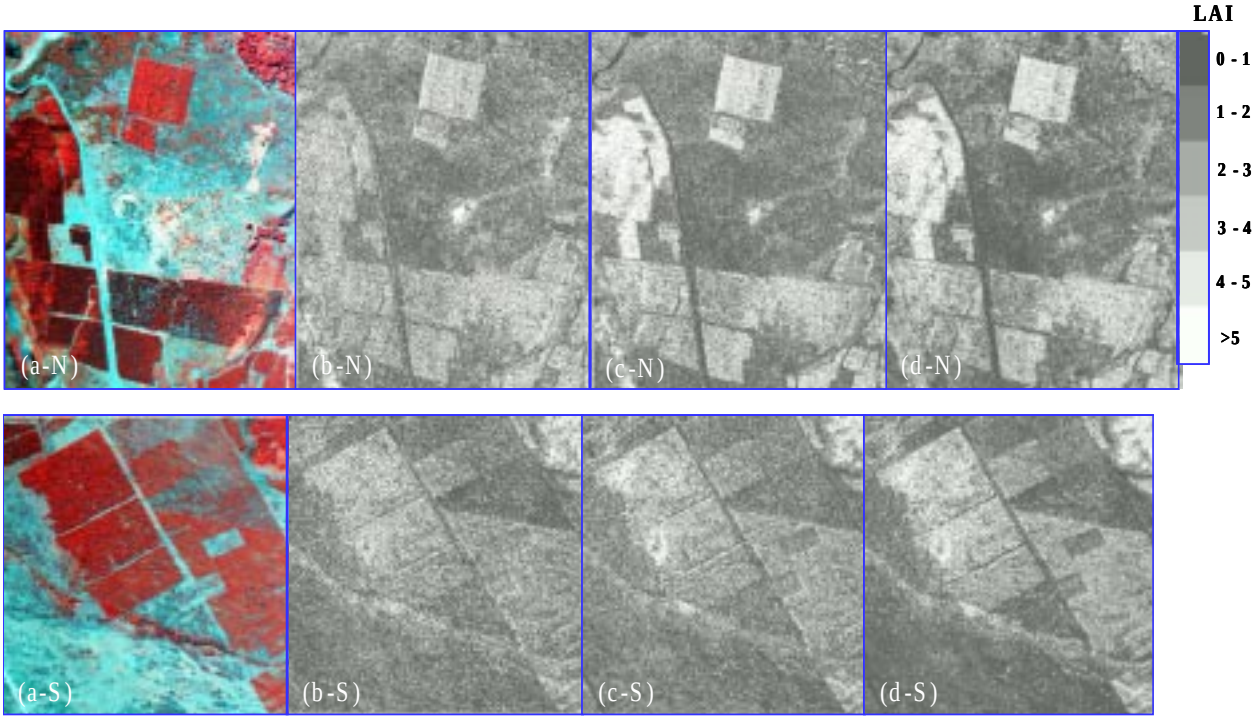

Figure 6. LAI mapping using three types of AVIRIS images. The upper four subimages are from the north site and the lower four subimages from the south site. (a-N, a-S) False color composite (AVIRIS bands 45, 24, 12); (b-N, b-S) LAI mapping with original radiance; (c-N, c-S) with corrected radiance; and (d-N, d-S) with retrieved surface reflectance data.

simplified radiative transfer model for three parameters of the path radiance, the Sun-surface-sensor two transmittance, and the spherical albedo of atmosphere, followed by using the ground spectroradiometric measurements to improve the retrieved surface reflectance from the AVIRIS images. The CR images were obtained by simply deducting path radiance from the OR images. A 10-term LAI prediction model for each type of the data was constructed to predict pixel-based LAI value. Finally, the pixel-based LAI values were used to make LAI maps for all the three types of images.

The results indicate that the LAI mapped with SR is the most reasonable among those derived from the three types of data. The worst LAI map is from OR. According to the results of correlation analysis, the SR data type generated the greatest correlation coefficients with measured LAI. In general, we conclude that the retrieved surface reflectance data is more effective for forest LAI estimation compared to the other two types of data. Additional field LAI measurements may be needed to test the 10-term prediction models for LAI estimation.

ACKNOWLEDGEMENTS

This research was partially supported by a NASA EO-1 science validation grant (NCC5-492) and field support provided by the forest plantation inventory section of the agricultural department of the government of Argentina. Assistance in field work by Mirta Rosa Larrieu, Gillsermo Defossé, Florencia Farias, and Maria Cristina Frugoni is appreciated.

REFERENCES

Berk, A., G. P. Anderson, P. K. Acharya, J. H. Chetwynd, L. S. Bernstein, E. P. Shettle, M. W. Matthew, and S. M. Adler-Golden, 2000, *MODTRAN4 User's Manual,* Air Force Research Laboratory, Hanscom AFB, MA, pp. 1-93.

Chen, J. and J. Cihlar, 1996, "Retrieving Leaf Area Index of Boreal Conifer Forests Using Landsat TM images," *Remote Sens. Environ*., vol. 55, pp. 153-162.

Curran, P. J., 1989,"Remote Sensing Of Foliar Chemistry," *Remote Sens. Environ*., vol. 30, pp. 271-278.

Curran, P. J., J. A. Kupiec, and G. M. Smith, 1997, "Remote Sensing The Biochemical Composition of A Slash Pine Canopy," *IEEE Transactions on Geoscience and Remote Sensin*g, vol. 35, no. 2, pp. 415-420.

Elvidge, C. D., and F. P. Portigal, 1990, "Change Detection in Vegetation Using 1989 AVIRIS Data," In *Proceedings of SPIE: Imaging Spectroscopy of the Terrestrial Environmen*t, vol. 1298, pp. 178-189.

Fassnacht, K. S., S. T. Gower, M. D. MacKenzie, E. V. Nordheim, and T. M. Lillesand, 1997, "Estimating the Leaf Area Index of North Central Wisconsin Forests Using the Landsat Thematic Mapper," *Remote Sens. Environ*., vol. 61, pp. 229-245.

Gao, B. C., K. B. Heidebrecht, and A. F. H. Goetz, 1993, "Derivation of Scaled Surface Reflectances from AVIRIS Data," *Remote Sensing of Environmen*t, vol. 44, pp. 165-178.

Gobron, N., B. Pinty, and M. M. Verstraete, 1997, "Theoretical Limits to the Estimation of the Leaf Area Index on the Basis of Visible and Near-Infrared Remote Sensing Data," *IEEE Trans. Geosci. Remote Sensin*g, vol. 35, pp. 1438-1445.

Goetz, A. F. H., J. W. Boardman, B. Kindel, and K. B. Heidebrecht, 1997, "Atmospheric Corrections: On Deriving Surface Reflectance from Hyperspectral Images," In *Proceedings of SPIE: Imaging Spectrometry II*I, vol. 3118, pp. 14-22.

Gong, P., R. Pu, and J. R. Miller, 1992, "Correlating Leaf Area Index of Ponderosa Pine with Hyperspectral CASI Data," *Canadian Journal of Remote Sensin*g, vol. 18, pp. 275-285.

Gong, P., R. Pu, and J. R. Miller, 1995, "Coniferous Forest Leaf Area Index Estimation along the Oregon Transect Using Compact Airborne Spectrographic Imager Data," *P. E. & R. S*., vol. 61, no. 9, pp.1107-1117.

Green, R. O., 1992, "Retrieval of Reflectance from Calibrated Radiance Imagery Measured by The Airborne Visible Infrared Imaging Spectrometer (AVIRIS) for Lithological Mapping," *Imaging Spectroscopy: Fundamentals and Prospective Application,* pp. 61-71.

Green, Robert O, M. L. Eastwood, C. M. Sarture, T. G. Chrien, M. Aronsson, B. J. Chippendale, J. A. Faust, B. E. Pavri, C. J. Chovit, M. Solis, M. R. Olah, and O. Williams, 1998, "Imaging Spectroscopy and the Airborne Visible/Infrared Imaging Spectrometer (AVIRIS)," *Remote Sens. Environ*., vol. 65, pp.227-248.

Hu, B, K. Inannen, and J. R. Miller, 2000, "Retrieval of Leaf Area Index and Canopy Closure from CASI Data over the BOREAS Flux Tower Sites," *Remote Sens. Enviro*n., vol. 74, pp. 255-274.

Jacquemoud, S., S. L. Ustin, J. Verdebout, G. Schmuck, G. Andreoli, and B. Hosgood, 1996, "Estimating Leaf Biochemistry Using the PROSPECT Leaf Optical Properties Model," *Remote Sens. Environ.*, vol. 56, pp. 194-202.

Jia, X. and J. A. Richards, 1999, "Segmented Principal Components Trasformation for Efficient Hyperspectral Remote-Sensing Image Display and Classification," *IEEE Transactions on Geoscience and Remote Sensing*, vol. 37, no. 1, pp. 538-542.

Miller, J. R., Hare, E. W., and Wu, J., 1990, "Quantitative Characterization of the Vegetation Red Edge Reflectance. 1. An Inverted-Gaussian Reflectance Model," *International Journal of Remote Sensing*, vol. 11, pp. 1775-1795.

Qu, Z., A. F. H. Goetz, and K. B. Heidebrecht, 2001, High-accuracy atmosphere correction for hyperspectral data (HATCH), 2000, *AVIRIS 2000 Workshop Proceedings*, http://popo.jpl.nasa.gov/docs/workshops/00_docs/tos_html, pp. 1-8.

Richter, R., 1992, "Atmospheric Correction of Imaging Spectrometer Data," *Imaging Spectroscopy: Fundamentals and Prospective Application*, pp. 259-266.

Running, S. W., R. R. Nemani, D. L. Peterson, L. E.Band, D. F. Potts, L. L. Pierce, and M. A. Spanner, 1989, "Mapping Regional Forest Evapotranspiration and Photosynthesis by Coupling Satellite Data with Ecosystem Simulation," *Ecology*, vol. 70, no. 4, pp. 1090-1101.

Spanner, M. A., L. Jphnson, J. R., R. McCreight, J. Freemantle, J. Runyon, and P. Gong, 1994, "Remote Sensing of Seasonal Leaf Area Index across the Oregon Transect," *Ecological Applications*, vol. 4, pp. 258-271.

Strum, B, 1992, "Atmospheric and Radiometric Corrections for Imaging Spectroscopy," *Imaging Spectroscopy: Fundamentals and Prospective Application*, pp. 47-60.

Tanré, D., C. Deroo, and P. Duhaut et al., 1986, "Simulate the Satellite Signal in the Solar Spectrum (5S)," *User's Guide*, Laboratory d'Optique Atmospherique, U. S. T. de Lille, 59655 Villeneuve D'ascq, France.

Vane, Gregg and Alexander F. H. Goetz, 1993, "Terrestrial Imaging Spectrometry: Current Status, Future Trends," *Remote Sens. Environ.*, vol. 44, pp. 117-126.

Welles, J. M., and J. M. Norman, 1991, "Instrument for Indirect Measurement of Canopy Architecture," *Agron. J.*, vol. 83, pp. 818-825.

White, J. D., S. W. Running, R. Nemani, R. E. Keane, and K. C. Ryan, 1997, "Measurement and Remote Sensing of LAI in Rocky Mountain Montane Ecosystems," *Can. J. For. Res.*, vol. 27, pp. 1714-1727.